Electrons and phonons in YbC_6: Density functional calculations and angle-resolved photoemission measurements

I. I. Mazin
Center for Computational Materials Science, Naval Research Laboratory, Washington, DC 20375, USA

S. L. Molodtsov
Institut für Festkörperphysik, TU Dresden, D-01062 Dresden, Germany
(Received 17 March 2005; published 14 November 2005)

The electronic structure and selected zone-center phonons in Yb graphite intercalation compound (YbC_6) are investigated theoretically using density functional calculations and the local density approximation (LDA) +U approach for Coulomb correlations in the *f* shell. We find that both in the LDA and LDA+U approach the Yb *f* states are fully occupied providing no evidence for mixed-valent behavior. The obtained theoretical results are in good agreement with photoemission experiments. The 4*f* states are considerably hybridized both with the Yb 5*d* and C 2*p* states resulting in a non-negligible admixture of Yb *f* at the Fermi level. Soft Yb phonons, given a noticeable presence of the Yb states at the Fermi level, are probably responsible for the superconductivity recently reported in YbC_6.

DOI: 10.1103/PhysRevB.72.172504 PACS number(s): 74.78.−w, 71.20.−b, 71.18.+y

For a long time graphite intercalation compounds (GICs) have been attracting substantial attention due to their layered quasi-two-dimensional (2D) structure and the resulting large anisotropy of their electric and electronic properties.[1,2] Some of GICs are known to be superconducting at low temperatures.[3] A renewed interest in superconducting phenomena in intercalated graphites is due to the recent discoveries of superconductivity in MgB_2 and B_xC, electronically related to graphite.[4] An interesting example of graphite intercalation compounds is YbC_6. First, it is one of the only four known bulk intercalations with 4*f* metals: YbC_6, EuC_6, SmC_6, and TmC_6 (Ref. 5) which may indicate that *f* electrons play a certain role in bonding in these compounds. Likewise, YC_6 has not been synthesized so far, although Y behaves similar to lanthanides in systems with localized *f* electrons (cf. high-T_c cuprates). Last but not least, very recently superconductivity was discovered in YbC_6.[6]

Yb is known to form mixed-valent compounds,[7] so one may think mixed-valent physics is operative in YbC_6 as well. Therefore it is of interest to investigate the electronic structure of YbC_6 numerically and experimentally. Should a good agreement between the theory and experiment be established, the former can be used to gain some insight into the possible mechanism for superconductivity. Experimentally, Yb valence in the above compound can be obtained by recording the Yb 4*f* photoemission (PE) spectra. Due to the large Coulomb-correlation energy, the energy positions of the PE signals for 4*f* configurations with different electron occupations are shifted by several eV with respect to each other. Therefore the contributions to the PE from different 4*f* configurations can easily be discriminated.[8] From the intensity ratio of these contributions the information about the valence can be derived.

In this paper we present *ab initio* calculations of the electronic structure of YbC_6 using both the local density approximation (LDA) and LDA+U approach, which accounts for Coulomb correlations inside the *f* shell. The calculated energies for the Yb 4*f* states are in good agreement with the results of photoemission experiments giving no evidence for the mixed-valent behavior. We also report first principles calculations of selected zone center phonons. We find soft Yb-derived phonons to be likely responsible for the superconductivity reported in YbC_6.

For the calculations, we used experimental crystal structure $P6/mmc$, with C occupying 12*i* and Yb 2*d* positions, with the lattice parameters $a=4.32$ Å and $c=9.1$ Å (Fig. 1). A full potential linear augmented plane wave method (LAPW) was used[9] with the following setup: The APW sphere radii were taken as 2.5 and 1.3 bohr, the cutoff parameter $RK_{\max}=7$, and local orbitals were used for Yb *s* and *p* and for C *s*, to reduce the linearization error, and to improve convergence in $RK_{\max}$. The linear tetrahedron method was employed for the Brillouin zone (BZ) integration, with the **k** mesh up to $11\times11\times4$ divisions. Spin-orbit coupling was included on the second variational basis.[9] The Ceperley-Alder exchange-correlation potential was used in the LDA part of the calculations. Finally, Hubbard correlations in the *f* shell were taken into account using the fully localized[10] version of the LDA+U formalism, with the parameters $U=0.4$ Ry and $J=0.05$ Ry.

These parameters were estimated by modifying occupation numbers in the quasiatomic loop in a LMTO (linear muffin-tin orbital) program. This is equivalent to a simplified version of the constraint LDA method,[11] which, in turn, is based on a definition of *U* as the derivative of the position of the atomic level with respect to the appropriate occupation number, e.g., $U_f=d\epsilon_{f\uparrow}/dn_{f\downarrow}$. The LMTO method[12] provides a natural gauge for $\epsilon_{f\sigma}$, the band center parameter $c_\nu(L=3)$, and an easy way to define $n_{f\sigma}$ as the charge of the *f* character inside the corresponding atomic sphere. The complications and ambiguity start when one defines the constraint keeping $n_{f\sigma}$ at a prescribed value. The standard recipe is to treat a supercell, centered around the considered atom, and perform full self-consistent calculations with an additional constraining potential, acting only on the *f* electrons, adjusted at each iteration so that $n_{f\sigma}$ would keep the prescribed value. The

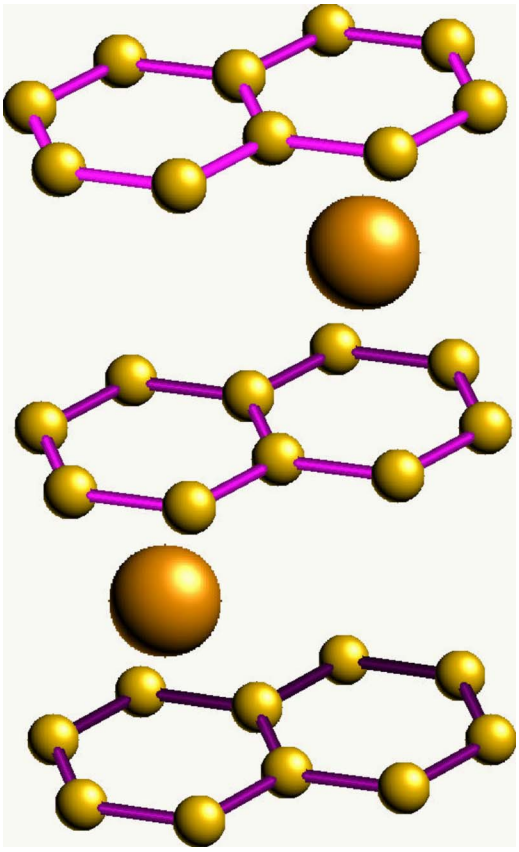

FIG. 1. (Color online) Crystal structure of YbC_6. Large spheres denote Yb and small spheres denote C. One unit cell (two formula units) is shown.

charge of all other electrons is allowed to flow in or out the central atomic sphere. We, instead, effectively, perform atomic calculations by changing the self-consisted occupation of the *f* states to the desired value and redistributing the extra charge over all other angular momenta in the same cell. Then we rerun the inner pseudoatomic loop, present in all LMTO packages, to allow all radial wave functions to screen the extra *f* charge. The advantage of this technique is it does not require any additional programming and the computational time is negligible. The main disadvantage is that, since the screening charge is confined in the same atomic sphere, the resulting U is usually somewhat overscreened. J can be computed in the same way, using the formula $J_f = d(\epsilon_{f\uparrow} - \epsilon_{f\downarrow})/d(n_{f\uparrow} - n_{f\downarrow})$. Since no net charge flow is involved, in this case the approach is more accurate.

The band structure calculated within the LDA+U scheme is shown in Fig. 2. Probably the most intriguing observation is that all *f* states appear to be fully occupied, giving evidence to firmly divalent Yb. This seems to be related to the fact that a straight LDA calculation (not shown), without any account of intra-*f*-shell Hubbard-type correlations, still places all *f* bands below the Fermi level, although, of course, much higher in energy than in LDA+U. As a result, when the LDA+U correction is applied to the LDA bands, it is of the same sign (negative) for all *f* states. We did check, though, that starting the LDA+U calculations from a trivalent Yb ion we still converge to the divalent solution.

The spin-orbit interaction splits the *f* states into two manifolds, located 1.10 and 2.30 eV below the Fermi level (E_F). The corresponding total electronic density of states (DOS) with two strong peaks originating in the 4*f* states is demonstrated in Fig. 3. Calculated positions of the 4*f* states in lanthanide systems depend very much on the specific choice of U and J values, which are often used as fitting parameters to achieve better correspondence with the experimental data. It is worth noting that in the present study the U and J values were estimated from the first principles and no attempts were done to fit or tune these parameters.

Most importantly, the qualitative prediction of purely divalent Yb in Yb-GIC is unambiguously supported by the PE data. Figure 4 depicts a series of angle-resolved PE spectra for Yb-GIC.[13] Most of the features are related to graphite bands and are discussed in detail in Ref. 13. If we concentrate, however, on the two nondispersive peaks, marked by two thin lines through the spectra in Fig. 4, we realize that these are a contribution into the PE signal from the Yb 4*f* electrons. They are found at 1.14 and 2.41 eV binding ener-

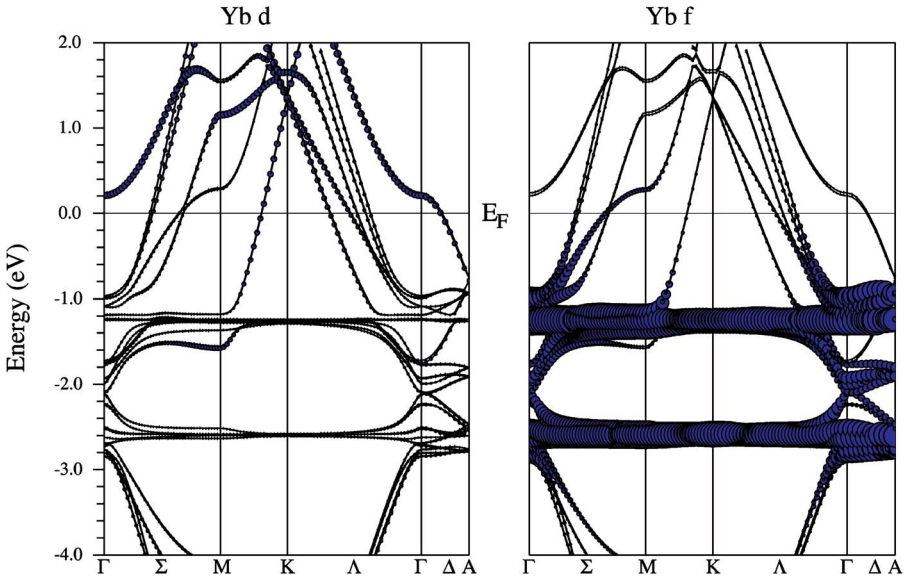

FIG. 2. (Color online) LDA+U band structure of YbC_6. The left panel shows the partial Yb-*d* character, and the right panel Yb-*f* character.

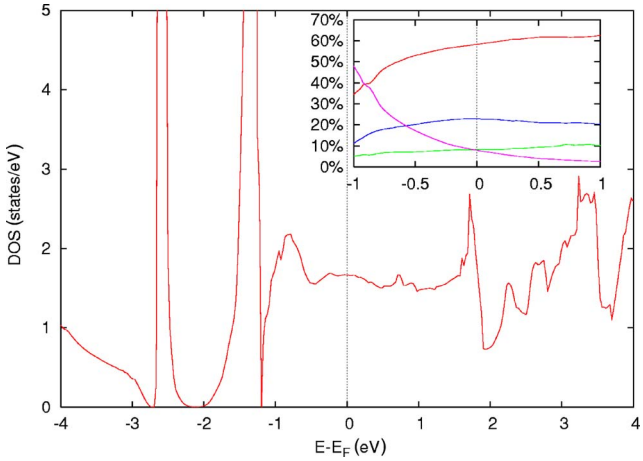

FIG. 3. (Color online) Electronic density of states of YbC_6. The main graph shows the total DOS on a per-formula-unit basis and the inset shows, in the order from the lowest to highest DOS at $E-E_F=1$ eV (that is from purple to green to blue to red), the partial contribution of Yb f, Yb d, C p character inside the corresponding APW spheres and the contribution of interstitial states.

gies (BEs). If the divalent $4f$ component of the final-state PE multiplet was observed at the Fermi energy, it would have indicated that the final-state multiplet is energetically degenerate with the ground state, consistent with a homogeneous mixed-valent behavior of the system. In the present case, the divalent signal is observed too far from E_F to anticipate the mixed-valent properties of the compound. Correspondingly,

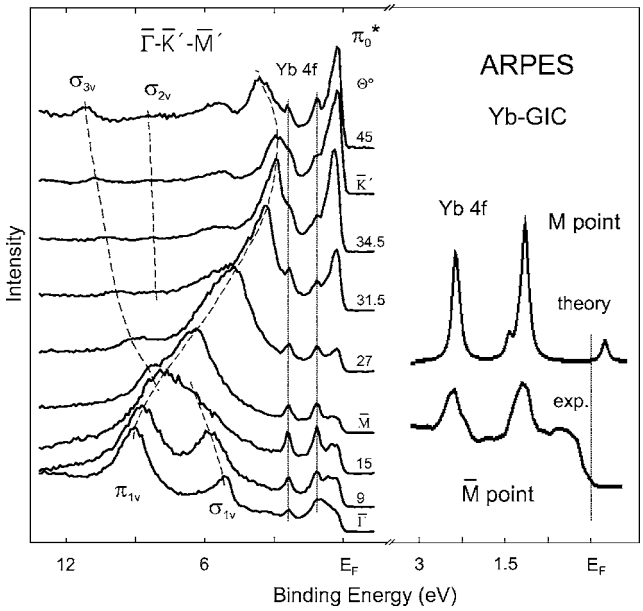

FIG. 4. (Left) Angle-resolved PE spectra (ARPES) of the Yb-GIC taken along the $\bar{\Gamma}$-$\bar{K}'$-$\bar{M}'$ direction in the 2D graphene Brillouin zone (this corresponds to the $\bar{\Gamma}$-$\bar{M}$-$\bar{\Gamma}$-$\bar{M}$ direction in the surface BZ of the Yb-GIC; see Ref. 13 for details) at different polar angles Θ. (Right) Comparison between the local f DOS in the vicinity of the M point in the bulk BZ of the Yb-GIC and the angle-resolved PE spectrum sampling the $\bar{M}$ region. Note that the experimentally probed point has a nonzero $\mathbf{k}_z$, as opposed to the M point.

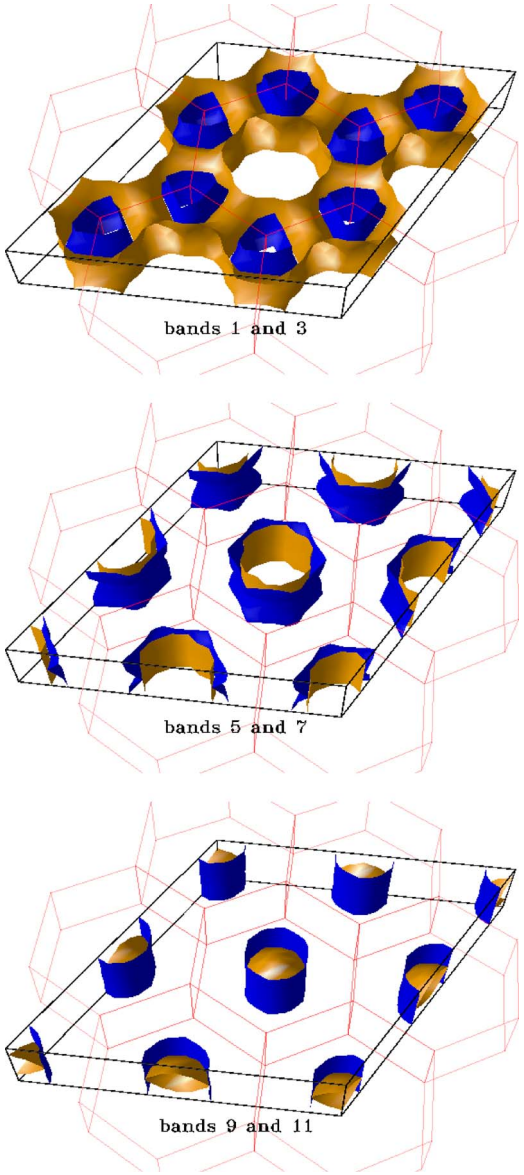

FIG. 5. (Color online) LDA+U Fermi surface of YbC_6. The band with the lower index is blue (darker in grey scale).

no traces of a trivalent signal in the region of 5–12 eV BE,[8] which one would expect for a mixed-valent system, are seen in the photoemission spectra.

The experimentally obtained binding energies of the divalent $4f$ contributions are in excellent agreement with the theoretical values. Not only energies, but also line shapes of the DOS and PE spectra are in agreement with each other. In the right panel of Fig. 4 we compare the angle-resolved PE spectrum sampling electronic states in the region of the $\bar{M}$ point in the surface BZ of the Yb-GIC with the local f DOS (spectral function) calculated around the M point. The calculated local DOS was broadened with a Lorentzian (70 meV) to account for finite lifetime effects. Good correspondence between the theoretical and experimental data is evident in the figure.[14] In fact, the agreement is better than one expects given the approximations used. Nevertheless, even though such level of accuracy is likely fortuitous, this clearly indi-

cates that the underlying physics is correctly described by the calculations, and, importantly, that the derived values of U and J are reasonably correct.

We shall now discuss the calculated electronic structure in more detail. Even in the vicinity of the Fermi level there is noticeable admixture of the f character (Fig. 2), indicating that the valence state of the f electrons plays an important role in transport properties in this material. There are 12 bands crossing the Fermi level. However, spin-orbit splitting at E_F is very small, so that one can safely speak about six distinct Fermi surfaces, corresponding to bands 1, 3, 5, 7, 9, and 11, shown in Fig. 5. An easy way to make the correspondence between the Fermi surfaces and the bands plotted in Fig. 2 is to count them from K to Γ: the only band crossing the Fermi level between K and M is band 1(2), while the state at approximately 0.2 eV at Γ is band 11(12). Bands 1, 5, 7, and 9 are quasi-2D, while bands 3 and 11 have considerable dispersion along the z direction. It is instructive to look at the element specific character of these bands. Band 11, forming elliptical pockets around Γ, has more Yb character than C, and namely Yb $d_{z^2-r^2}$ character. Not surprisingly, this is the band that is most dispersive in the z direction. Bands 5–8 have predominantly C p_z origin (band 5 with a considerable hybridization with Yb f), while bands 1 and 3 show only small contributions within either C or Yb muffin-tin spheres, but rather in the interstitial areas, thus being mostly free-electron-like.

While at the Fermi level most of the DOS (inset in Fig. 3) comes from the extended states in the interstitial region, there is a non-negligible share of the Yb f states, which rapidly grows with increasing BE. Contribution of the Yb d states (mostly $d_{z^2-r^2}$ symmetry) is also considerable. This indicates that Yb phonons may play a role in superconductivity. The total density of states at the Fermi level is $N(E_F)$ $=1.7$ states/(eV formula). The average Fermi velocity in- and out-of-plane, respectively, is 4.8×10^7 and 2.7×10^7 cm/s. The corresponding components of the plasma frequency are 6.2 and 3.6 eV, implying, in the constant scattering rate approximation, a resistivity anisotropy of about 3.

The large unit cell of YbC_6 allows for multiple zone-center modes, which in principle can be computed by the frozen phonon method. 24 modes corresponding to in-plane motion of C are expected to be very hard, since C $p_{x,y}$ orbitals are removed from the Fermi level (as opposed, for instance, to MgB_2). Indeed, we calculated the frequency of the fully symmetric A_{1g} mode to be 1540 cm^{-1}. Most of the 12 out-of plane C modes, by symmetry, have zero deformation potential at Γ and thus do not couple with electrons, while the E_g mode lowers the symmetry to triclinic and is prohibitively difficult to compute accurately. Thus we are left with the 6 Yb modes, of which the three even modes correspond to a double degenerate E_{2g} phonon involving displacements of Yb parallel to the graphite plane, and a B_{1g} one, corresponding to Yb displacements along c. These modes are rather soft; our calculations place them at 77 and 153 cm^{-1}, respectively. Unfortunately, the electron-phonon coupling exactly at the zone center is strongly suppressed by symmetry for these three modes. If the alternating Yb planes were not shifted with respect to each other, cf. Fig. 1, it would be forbidden, so in the actual structure it is suppressed to the extent of the weakness of Yb–Yb interaction. However, their low frequency and considerable presence of Yb character at the Fermi level suggest that coupling of these and similar modes, when integrated over the Brillouin zone, may be sufficient to explain superconductivity in YbC_6.

Work at the Naval Research Laboratory was supported by the Office of the Naval Research. The experimental part was supported by the Deutsche Forschungsgemeinschaft, SFB 463 (TP B16).

[1] *Intercalation Compounds of Graphite*, edited by F. L. Fogel and A. Herold (Elsevier Sequoia, Lausaune, 1977).

[2] *Intercalation in Layered Materials*, edited by M. S. Dresselhaus, *NATO ASI Series B: Physics Vol. 148* (Plenum Press, New York, 1986).

[3] N. B. Hannay, T. H. Geballe, B. T. Matthias, K. Andres, P. Schmidt, and D. MacNair, Phys. Rev. Lett. **14**, 225 (1965).

[4] I. I. Mazin and V. P. Antropov, Physica C **385**, 49 (2003).

[5] M. El Makrini, D. Guérard, P. Lagrange, and A. Hérold, Physica B **99**, 481 (1980); M. S. Dresselhaus and G. Dresselhaus, Adv. Phys. **30**, 139 (1981).

[6] T. E. Weller, M. Ellerby, S. S. Saxena, R. P. Smith, and N. T. Skipper, Nat. Phys. **1**, 39 (2005).

[7] *Valence Fluctuations in Solids*, edited by L. M. Falicov, W. Hanke, and M. B. Maple (North-Holland, Amsterdam, 1981).

[8] S. Wieling, S. L. Molodtsov, Th. Gantz, J. J. Hinarejos, C. Laubschat, and M. Richter, Phys. Rev. B **58**, 13219 (1998); S. Wieling, S. L. Molodtsov, Th. Gantz, and C. Laubschat, *ibid.* **64**, 125424 (2001).

[9] P. Blaha, K. Schwarz, G. K. H. Madsen, D. Kvasnicka, and J. Luitz, *Wien*, 2002, an Augmented Plane Wave+Local Orbitals Program for Calculating Crystal Properties (Karlheinz Schwarz, Techn. Universität Wien, Austria).

[10] A. G. Petukhov, I. I. Mazin, L. Chioncel, and A. I. Lichtenstein, Phys. Rev. B **67**, 153106 (2003).

[11] V. I. Anisimov and O. Gunnarsson, Phys. Rev. B **43**, 7570 (1991).

[12] O. K. Andersen, Phys. Rev. B **12**, 3060 (1975).

[13] S. L. Molodtsov, Th. Gantz, C. Laubschat, A. G. Viatkine, J. Avila, C. Casado, and M. C. Asensio, Z. Phys. B: Condens. Matter **100**, 381 (1995); S. L. Molodtsov, C. Laubschat, M. Richter, Th. Gantz, and A. M. Shikin, Phys. Rev. B **53**, 16621 (1996).

[14] The PE intensity close to E_F is due to non-f states, most likely C-derived band 1 (Fig. 5), which is somewhat dispersive along $\mathbf{k}_z$ and appears at -1.1 eV at M ($\mathbf{k}_z=0$), but at -0.75 eV at L ($\mathbf{k}_z=\pi/c$). The occupied tail of the band found at about 0.2 eV in the M point (Fig. 2) may also contribute to the Fermi-level intensity. As usual in ARPES experiments, there are in addition contributions from other bands all over the BZ caused by indirect transitions.